Adipose Tissue Overexpression of Vascular Endothelial Growth Factor Protects Against Diet-Induced Obesity and Insulin Resistance

Ivet Elias,[1,2,3] Sylvie Franckhauser,[1,3] Tura Ferré,[1,3] Laia Vilà,[1,2,3] Sabrina Tafuro,[1,3†] Sergio Muñoz,[1,2,3] Carles Roca,[1,2,3] David Ramos,[1,4] Anna Pujol,[1,2,3] Efren Riu,[1,2,3] Jesús Ruberte,[1,3,4] and Fatima Bosch[1,2,3]

During the expansion of fat mass in obesity, vascularization of adipose tissue is insufficient to maintain tissue normoxia. Local hypoxia develops and may result in altered adipokine expression, proinflammatory macrophage recruitment, and insulin resistance. We investigated whether an increase in adipose tissue angiogenesis could protect against obesity-induced hypoxia and, consequently, insulin resistance. Transgenic mice overexpressing vascular endothelial growth factor (VEGF) in brown adipose tissue (BAT) and white adipose tissue (WAT) were generated. Vessel formation, metabolism, and inflammation were studied in VEGF transgenic mice and wild-type littermates fed chow or a high-fat diet. Overexpression of VEGF resulted in increased blood vessel number and size in both WAT and BAT and protection against high-fat diet–induced hypoxia and obesity, with no differences in food intake. This was associated with increased thermogenesis and energy expenditure. Moreover, whole-body insulin sensitivity and glucose tolerance were improved. Transgenic mice presented increased macrophage infiltration, with a higher number of M2 anti-inflammatory and fewer M1 proinflammatory macrophages than wild-type littermates, thus maintaining an anti-inflammatory milieu that could avoid insulin resistance. These studies suggest that overexpression of VEGF in adipose tissue is a potential therapeutic strategy for the prevention of obesity and insulin resistance. ***Diabetes*** **61:1801–1813, 2012**

Obesity, an epidemic disease whose prevalence is increasing at an alarming rate, is a major risk factor for serious chronic diseases, including insulin resistance, type 2 diabetes, and cardiovascular disease (1,2). However, the mechanisms through which obesity leads to these metabolic complications are not fully understood. Adipose tissue mass increases during obesity, and to provide sufficient oxygen and nutrients to all cells, angiogenesis has to support adipose tissue growth (3). Several studies postulate that during obesity, this enlargement of the vascular network is not sufficient to supply enough oxygen to all adipocytes and local hypoxia occurs (4–7). It has been hypothesized that this insufficient adipose tissue blood flow may trigger insulin resistance via effects on inflammation, adipokine expression, and/or adipocyte differentiation (8–10).

Adipose tissue macrophages (ATMs) play an important role in the establishment of the chronic inflammatory state associated with obesity and its metabolic dysfunctions (11,12). Lumeng et al. (13) demonstrated in recent studies that ATMs from lean mice are M2 or "alternatively activated" macrophages, whereas ATMs from obese mice are predominantly M1 or "classically activated" macrophages. Whereas M2 macrophages present anti-inflammatory properties and are associated with angiogenesis and wound repair, M1 macrophages are associated with inflammation. The cross-talk among proinflammatory macrophages, adipocytes, and endothelial cells during obesity may aggravate the inflammatory state, resulting in increased secretion of proinflammatory molecules, including acute-phase reactants, procoagulant factors, cytokines, and chemokines (8,14,15). These factors can cause local and/or systemic insulin resistance in a paracrine, autocrine, and/or endocrine fashion.

We therefore hypothesized that an increase in adipose tissue angiogenesis may protect from obesity-induced hypoxia, and consequently, from inflammation and insulin resistance in this tissue. Vascular endothelial growth factor (VEGF) is a key factor involved in adipose tissue angiogenesis (16–18); however, its role and expression levels during obesity remain unclear (6,7,19). Thus, to determine the effects of an increase in VEGF levels in adipose tissue, transgenic mice overexpressing VEGF in WAT and BAT were obtained. Our results indicate that VEGF overexpression led to increases in vascularization and in the amount of M2 anti-inflammatory macrophages, which protected transgenic mice not only against high-fat diet (HFD)–induced obesity but also insulin resistance.

RESEARCH DESIGN AND METHODS

Animals. Transgenic mice expressing the *aP2/Vegf* chimeric gene were obtained by microinjection of oocytes from C57Bl6/SJL mice. Mice were kept in a pathogen-free facility (Servei d'Estabulació de Ratolins-Centre de Biotecnologia Animal i Teràpia Gènica) and maintained under a 12-h light–dark cycle at 22°C. Mice were fed ad libitum for 15 weeks with a chow diet (2018S Harlan Teklad, Madison, WI) or an HFD (TD88137 Harlan Teklad). When stated, mice were fasted for 16 h.

An indirect open circuit calorimeter (Oxylet, Panlab, Cornellà, Spain) was used to monitor oxygen consumption, carbon dioxide production, and locomotor activity in eight metabolic chambers simultaneously. Mice were individualized and acclimated to the metabolic chambers for 24 h, and data were collected every 15 min for 3 min in each cage. Data were taken from the light and dark cycle. The LE5007 system (Panlab) was used to measure blood pressure, and animals were kept in a restrainer and heated using the Heater

From the [1]Center of Animal Biotechnology and Gene Therapy, Universitat Autònoma de Barcelona, Bellaterra, Spain; the [2]Department of Biochemistry and Molecular Biology, Universitat Autònoma de Barcelona, Bellaterra, Spain; the [3]Centro de Investigación Biomédica en Red de Diabetes y Enfermedades Metabólicas Asociadas (CIBERDEM), Barcelona, Spain; and the [4]Department of Anatomy and Animal Health, School of Veterinary Medicine, Universitat Autònoma de Barcelona, Bellaterra, Spain.

Corresponding author: Fatima Bosch, fatima.bosch@uab.es.

Received 17 June 2011 and accepted 29 February 2012.

DOI: 10.2337/db11-0832

This article contains Supplementary Data online at http://diabetes.diabetesjournals.org/lookup/suppl/doi:10.2337/db11-0832/-/DC1.

†Deceased.

Scanner LE 5650/6 (Panlab). Animals were anesthetized and killed, and tissues of interest were excised and kept at −80°C or preserved with formalin until analysis. Animal care and experimental procedures were approved by the Ethics Committee in Animal and Human Experimentation of the Universitat Autònoma de Barcelona.

Gene expression analysis. For quantitative real-time PCR analysis, total RNA was extracted from different tissues using TriPure isolation reagent (Roche, Mannheim, Germany) for nonfat tissues and QIAZOL (Qiagen, Hilden, Germany) for fat tissues, and Rneasy Mini Kit (Qiagen). Total RNA (1μg) was retrotranscribed using the SuperScript VILO cDNA Synthesis Kit (Invitrogen, Carlsbad, CA). Real-time PCR was performed in a SmartCycler II (Cepheid, Sunnyvale, CA) using EXPRESS 2× qPCR SuperMix (Invitrogen). Oligonucleotide sequences were: *Vegfa*$_{164}$–FW: 5′-AGACAGAACAAAGCCAGAAATCAC-3′, RV: 5′-CACGTCTGCGGATCTTGGAC-3′; *Pecam-1*–FW: 5′-CTGGTGCTCTATGCAAGCCTC-3′, RV: 5′-CGGTGCTGAGACCTGCTTT-3′; *Kdr*–FW: 5′-AGCTTGGCTCACAGGCAACAT-3′, RV: 5′-TGGCCCGCTTAACGGTCCGTA-3′; *Srebf1*–FW: 5′-GGAGCCATGGATTGCACATT-3′, RV: 5′-GCTTCCAGAGAGGAGGCCAG-3′; *Fasn*–FW: 5′-GCTGCGGAAACTTCAGGAAAT-3′, RV: 5′-AGAGACGTGTCACTCCTGGAC-3′; *Il10*–FW: 5′-CTATGCTGCCTGCTCTTACTG-3′, RV: 5′-AACCCAAGTAACCCTTAAAGTC-3′; *Arg1*–FW: 5′-GGAATCTGCATGGGCAACCTGTGT-3′, RV: 5′-AGGGTCTACGTCTCGCAAGCCA-3′; *Hif1a*–FW: 5′-GACTAGACAAAGTTCACCTGAGA-3′, RV: 5′-CGCTATCCACATCAAAGCAA-3′; *Cxcl12*–FW: 5′-TGCATCAGTGACGGTAAACCA-3′, RV: 5′-TTCTTCAGCCGTGCAACAATC-3′; *Lep*–FW: 5′-GAGACCCCTGTGTCGGTTC-3′, RV: 5′-CTGCGTGTGTGAAATGTCATTG-3′; *Adipoq*–FW: 5′-TGTTCCTCTTAATCCTGCCCA-3′, RV: 5′-CCAACCTGCACAAGTTCCCTT-3′; and *36B4*–FW: 5′-TCCCACCTTGTCTCCAGTCT-3′, RV: 5′-ACTGGTCTAGGACCCGAGAAG-3′.

Western blot analysis. Tissues were homogenized in protein lysis buffer as previously described (20). Primary antibodies were anti-VEGF (Abcam ab46154, Cambridge, U.K.); anti–hypoxia-inducible factor (HIF)-1α (Abcam ab1); anti-uncoupling protein (UCP)1 (Abcam ab10983); anti-peroxisome proliferator–activated receptor γ coactivator (PGC)-1α (Chemicon AB3242, Millipore, Billerica, MA); anti-Akt (Cell Signaling 9272, Danvers, MA) and anti–phospho-Akt (Ser473) (Cell Signaling 9271).

Immunohistochemical and morphometric analysis. Tissues were fixed for 24 h in formalin, embedded in paraffin, and sectioned. For immunohistochemical detection, sections were deparaffinized and incubated overnight at 4°C with antibody against Mac-2 (Cederlane CL8942AP, Ontario, Canada) or against VEGF (Abcam ab46154), washed with PBS three times for 5 min for each wash, incubated with the corresponding secondary antibodies, and revealed with ABC Complex (Vector Laboratories Ltd., Peterborough, U.K.). Sections were counterstained in Mayer's hematoxylin.

Measurement of the adipocyte area. A morphometric study of adipocytes size was performed in WAT sections stained with hematoxylin-eosin. Adipocytes area was determined as previously described (21). Four animals per group were used and at least 250 adipocytes per animal were analyzed.

Transmission electron microscopy analysis. WAT and BAT samples were processed as described elsewhere (22).

Fluorescein angiography. Mice were injected with 10 mL/kg fluorescein isothiocyanate–conjugated dextran solution (50 mg/mL; Sigma-Aldrich, St. Louis, MO). After 10 min, animals were killed and tissues were dissected and placed in formalin. Samples were incubated with rhodamine-phalloidin, placed on glass slides covered with mounting media for fluorescence (Vectashield, Peterborough, U.K.), and analyzed on a laser-scanning confocal microscope (Leica Mycrosystems, Wetzlar, Germany) at original magnification ×400. Each image represents an overlay of 20 images (WAT) or 30 images (BAT) separated by 1 μm. For morphometric analysis, the vessel area of 10 consecutive images was measured.

Hypoxyprobe staining. Hypoxyprobe staining was performed using the Hypoxyprobe-1 Kit (Hypoxyprobe Inc., Burlington, MA). Pimonidazole (60 mg/kg) was injected into mice via a tail vein 30 min before sampling. Samples were removed, fixed, and processed according to the manufacturer's instructions.

Glucose and insulin-tolerance tests. Glucose and insulin-tolerance tests were performed as previously described (20). Briefly, mice were given an intraperitoneal injection of glucose or insulin, and the glucose concentration was determined in blood samples at indicated time points.

Insulin signaling. To study insulin signaling, overnight fasted animals were anesthetized and quadriceps and a piece of epididymal adipose tissue were excised and frozen into liquid nitrogen. Immediately, mice were intraperitoneally injected with insulin (0.15 units/g body weight). Ten minutes later, other tissues were excised and frozen. Protein extracts of different samples were obtained for Western blot analysis.

Enzyme, metabolite, and hormone assays. Tissue triglyceride content was determined by extracting total lipids from liver, quadriceps, kidney, and heart samples with chloroform-methanol (2:1 vol/vol), as described by Carr et al. (23). Triglycerides, total cholesterol, and HDL cholesterol were quantified spectrophotometrically using an enzymatic assay kit (Horiba-ABX, Montpellier, France). Serum free fatty acids (FFAs) were measured by the acyl-CoA synthase and acyl-CoA oxidase methods (Wako Chemicals GmbH, Neuss, Germany). Serum glycerol concentration was determined enzymatically (Randox Laboratory, Crumlin, U.K.). All biochemical parameters were determined using a Pentra 400 Analyzer (Horiba-ABX). Glucose was determined using a Glucometer Elite analyzer (Bayer, Leverkusen, Germany), and insulin levels were measured using the Rat Insulin ELISA Kit (Crystal Chemical, Chicago, IL). Leptin concentration was determined using the Mouse Leptin ELISA Kit (Crystal Chemical). VEGF protein levels were measured using the Mouse VEGF ELISA Kit (Calbiochem, Darmstadt, Germany). Serum monocyte chemoattractant protein (MCP)-1 levels were determined using the Mouse MCP-1 ELISA Kit (eBioscience, San Diego, CA), and serum adiponectin levels were measured by mouse/rat RIA Kit (Millipore, Billerica, MA). MCP-1, interferon (IFN)-γ, interleukin (IL)-6, and tumor necrosis factor (TNF)-α WAT protein levels were measured by Luminex xMAP using Millipore reagents and instructions.

Isolation of the WAT stroma vascular fraction. WAT was excised and put in a tube containing PBS/BSA 0.5% solution (2 mL) at 37°C. The tissue was minced and digested at 37°C for 30 min by the addition of 1 mg/mL collagenase P from *Clostridium histolyticum* (Roche). The supernatant was filtered through a 30-μm pore filter (Partec CellTrics, Görlitz, Deutschland) to obtain a single cell suspension, and the filtrate was recollected in Falcon tubes. After the addition of PBS/BSA 0.5%, the filtrate was spun. Supernatant was eliminated, and the pellet was resuspended in RBC lysis buffer (eBioscience) and incubated for 5 min to break the erythrocytes. After addition of PBS/BSA 0.5% and a spin, the pellet was resuspended in 500 μL PBS/BSA 0.5%.

Flow cytometry. The stroma vascular fraction was incubated with specific antibodies: phycoerythrin (PE) anti-mouse cluster of differentiation (CD)11b (BD Pharmigen 557397, Franklin Lakes, NJ), PE/Cy7 anti-mouse CD11b (Biolegend 101216, San Diego, CA), PE anti-mouse CD11c (BD Pharmigen 557401), fluorescein isothiocyanate anti-mouse F4/80 (Biolegend 123107), AlexaFluor 488 anti-mouse CD301 (AdB Serotec MCA2391A488T, Düsseldorf, Germany), and PE/Cy5 anti-mouse major histocompatibility complex (MHC) II (Biolegend 107611). Flow cytometric analysis was performed on a FC500 MPL (Beckman Coulter) equipped with an argon ion laser (488 nm, 20-mW output) and a red helium-neon laser (633 nm, 20-mW output). Data were analyzed using FCS3 Express software (De Novo Software, Los Angeles, CA).

Isolation and culture of bone marrow–derived macrophages (BMDMs). BMDMs were prepared from the femur and tibia of mice. Cells were cultured with complete RPMI supplemented with macrophage colony-stimulating factor (Gibco, Invitrogen) for 7 days (24) and then treated with 100 ng/mL recombinant mVEGF (Cell Signaling) for 24 h before collection of the cells.

Statistical analysis. All values are expressed as the mean ± SEM. Differences between groups were compared by Student *t* test. Statistical significance was considered if $P < 0.05$.

RESULTS

Adipose-specific overexpression of VEGF leads to increased vessel density. Two transgenic mouse lines (L1 and L2) expressing VEGF under the control of the adipose-specific aP2 promoter were obtained. L1 showed a slight increase in VEGF expression levels (data not shown), whereas L2 showed a high increase and this line was further studied. After Northern blot analysis, a marked increase in total *Vegf* mRNA levels was detected in WAT and BAT but not in skeletal muscle or liver from transgenic animals (Fig. 1*A*). Moreover, *Vegf*$_{164}$ mRNA levels were highly increased in different WAT depots (epididymal, retroperitoneal, and subcutaneous) and in interscapular BAT of transgenic mice (Fig. 1*B*). This increase was parallel to an increase in VEGF protein levels detected by immunohistochemistry or by Western blot (Fig. 1*C* and *D*). However, no differences in VEGF serum levels were detected between groups, probably due to the retention of VEGF by the extracellular matrix (Fig. 1*E*).

Because VEGF is a potent activator of angiogenesis, the effects of VEGF overexpression on vascularization were analyzed. Macroscopic observation showed that WAT and BAT were reddish (Fig. 1*F*), suggesting increased blood flow in the adipose tissue of transgenic mice. After tail-vein dextran-conjugated fluorescein injection and phalloidin staining, WAT and BAT angiographies showed an increase in functional blood vessels in the transgenic mice (Fig. 1*G*).

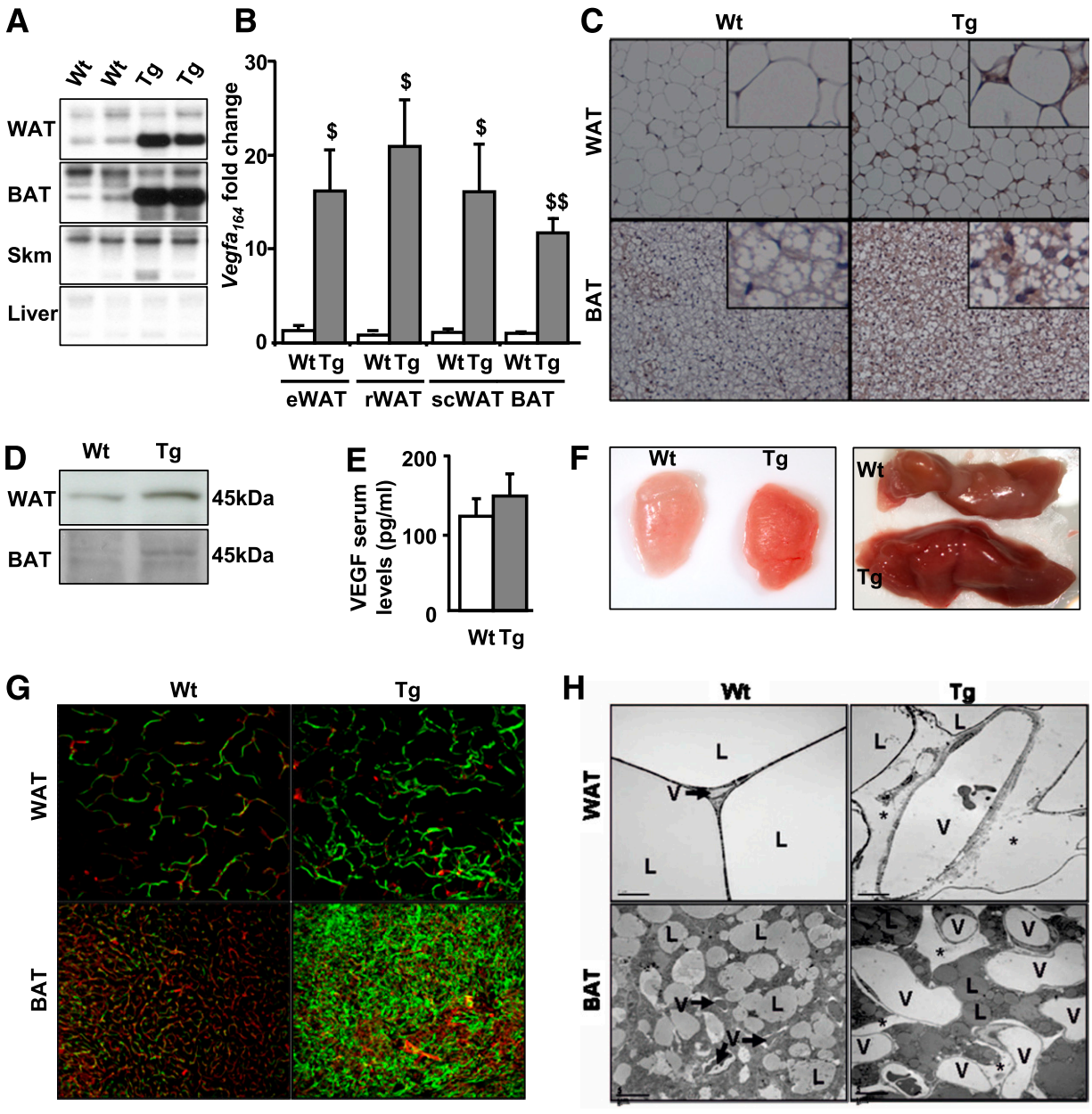

FIG. 1. Adipose-specific overexpression of VEGF led to increased vessel density. *A*: Representative Northern blot of epididymal WAT, BAT, skeletal muscle, and liver from wild-type (Wt) and transgenic (Tg) mice specific for *Vegfa*. *B*: *Vegfa*$_{164}$ expression was analyzed by quantitative real-time PCR in epididymal WAT (eWAT), retroperitoneal WAT (rWAT), subcutaneous WAT (scWAT), and BAT and was normalized by *36B4* expression. Data represent the mean ± SEM of at least seven animals per group. $$P < 0.05$ vs. Wt. $$$P < 0.01$ vs. Wt. *C*: VEGF immunohistochemistry in WAT and BAT. Figure shows representative images at original magnification ×200, with insets at higher magnification. *D*: Representative WAT and BAT Western blots blotted with an antibody against VEGF and showing a band of 45 KDa corresponding to VEGF. *E*: Serum VEGF levels were measured in serum samples by enzyme-linked immunosorbent assay. Data represent the mean ± SEM of at least seven animals per group. *F*: Representative macroscopic images of eWAT (*left*) and interscapular BAT (*right*). *G*: Images of WAT and BAT angiographies were taken after a tail-vein dextran-conjugated fluorescein injection (*green*) and in toto with phalloidin (*red*), by confocal microscopy (original magnification ×400). Angiographies represent an overlay of 20 images (WAT) or 30 images (BAT) separated by 1 μm. *H*: Transmission electron microscopy study of capillary ultrastructure in WAT and BAT (original magnification ×2,000). L, lipid droplets; V, blood vessels; *, edema. (A high-quality digital representation of this figure is available in the online issue.)

The vessel/adipocyte area in wild-type compared with transgenic mice related to adipocyte area was increased in epididymal (0.27 ± 0.08 and 1.16 ± 0.17%, $n = 4$; $P \leq 0.01$), retroperitoneal (0.24 ± 0.06 and 0.59 ± 0.10%, $n = 4$; $P \leq 0.05$), and subcutaneous (0.23 ± 0.05 and 0.47 ± 0.05%, $n = 4$; $P \leq 0.05$) fat depots. Moreover, the specificity of the increase in vessel density in epididymal, retroperitoneal, subcutaneous WAT and interscapular BAT was corroborated by *Pecam-1* and *Kdr* expression levels (Supplementary Fig. 1*A* and *B*).

Transmission electron microscopy showed that capillaries from transgenic WAT and BAT were highly dilated (Fig. 1*H*), suggesting increased blood flow and oxygen supply to surrounding cells. Some edema was observed, suggesting an effect of VEGF on vessel permeability, although no fenestrations and a similar number of vesicles were observed in BAT capillaries of transgenic mice (Supplementary Fig. 1*C* and *D*). Metabolic parameters were determined in 6- and 12-month-old mice, and no differences between wild-type and transgenic mice were observed (Supplementary Table 1).

Lower adiposity in aP2VEGF transgenic mice fed an HFD. To examine whether an increase in adipose tissue angiogenesis could protect against obesity-induced hypoxia and, consequently, avoid inflammation and insulin resistance, transgenic mice were studied under HFD conditions. After 15 weeks of the HFD, weight gain increased by 30% in wild-type mice but only by 10% in aP2VEGF transgenic mice (Fig. 2*A*), although food intake was similar between the groups (Fig. 2*B*). In parallel to weight gain, the WAT weight and the adipocyte mean size increases were greater in wild-type mice than in transgenic mice (Fig. 2*C* and *D*). The frequency distribution of the area of white adipocytes was also different between groups. Wild-type mice fed an HFD presented fewer small adipocytes and an increase in the number of large adipocytes (Fig. 2*E*). In contrast, transgenic mice fed an HFD only presented an increased number of intermediate-sized adipocytes (Fig. 2*E*). Therefore, the HFD-induced hypertrophy of adipocytes observed in wild-type mice was attenuated in transgenic mice overexpressing VEGF. In addition, local hypoxia in WAT was only detected in control mice fed an HFD, suggesting that transgenic mice did not develop hypoxia (Fig. 2*F*). Accordingly, the HFD increased mRNA and protein levels of the hypoxia-inducible transcription factor (*Hif1a*) in wild-type mice but not in transgenic mice (Fig. 2*G* and *H*). Thus, VEGF overexpression in adipose tissue protected transgenic mice from diet-induced obesity and local hypoxia.

Transgenic mice showed increased thermogenesis activity. Histologic analysis of BAT in mice fed the chow diet showed that the morphology of this tissue was altered in transgenic mice, probably due to the presence of high vascularization (Fig. 3*A*). In addition, the interscapular BAT weight was almost twofold higher in transgenic mice than in wild-type animals (Fig. 3*B*). In contrast, when fed an HFD, BAT weight increased only in wild-type animals (Fig. 3*B*), probably due to less lipid deposition in transgenic mice. Total UCP1 (Fig. 3*C*) and PGC-1α (Fig. 3*D*) protein levels increased significantly in BAT of transgenic mice fed an HFD compared with wild-type mice. Accordingly, the energy expenditure of HFD-fed transgenic mice during the dark cycle (activity phase) was higher than that of wild-type mice (Fig. 3*E*), without changes in spontaneous locomotor activity (Fig. 3*F*). Body temperature was also more elevated in transgenic mice fed a chow diet compared with wild-type mice (Fig. 3*G*). However, body temperature increased to the same extent in wild-type and transgenic mice fed an HFD (Fig. 3*G*). Altogether, these data suggest that transgenic mice have increased thermogenic activity.

Less fat accumulation in nonadipose tissues of transgenic mice. Liver histologic sections showed no morphologic alterations in transgenic mice fed a chow diet. When fed an HFD, wild-type mice showed increased lipid accumulation in hepatocytes compared with transgenic mice (Fig. 4*A* and *B*). Similarly, sterol regulatory element-binding protein-1c *(Srebf1)* and fatty acid synthase *(Fasn)* expression were both increased in wild-type animals fed an HFD but not in transgenic mice fed an HFD (Fig. 4*C* and *D*). No differences in triglyceride content in skeletal muscle, heart, and kidney were detected between groups fed a chow diet. On an HFD, triglyceride content in skeletal muscle increased to a greater extent in wild-type animals than in transgenic mice but remained unchanged in heart and kidney (Fig. 4*E*–*G*).

Lipid profile after an HFD. Wild-type animals fed an HFD presented increased serum FFA and glycerol, whereas transgenic mice had a similar increase in FFA but not in glycerol levels (Fig. 5*A* and *B*). This suggested differences in FFA re-esterification between wild-type and transgenic mice. Similarly, transgenic mice fed an HFD presented lower triglyceride levels than wild-type mice (Fig. 5*C*). Transgenic mice also showed a lower HFD-induced increase in total and HDL cholesterol levels than wild-type mice (Fig. 5*D* and *E*). The origin of these alterations is not known. No changes in blood pressure were observed in transgenic mice (Fig. 5*F*).

aP2VEGF transgenic mice are protected against diet-induced glucose intolerance and insulin resistance. Wild-type and transgenic animals fed a chow diet were normoglycemic, normoinsulinemic, and presented similar insulin sensitivity and glucose tolerance (Fig. 6). However, glucose and insulin levels significantly increased in wild-type mice fed an HFD but remained lower in transgenic mice (Fig. 6*A* and *B*). An intraperitoneal insulin-tolerance test showed that insulin response was blunted in HFD-fed wild-type mice, whereas glucose levels were reduced by 40% in transgenic mice, indicating that they remained insulin-sensitive (Fig. 6*C*). In addition, wild-type mice fed an HFD presented impaired glucose tolerance whereas transgenic mice showed preserved glucose response (Fig. 6*D*). Accordingly, in adipose tissue and skeletal muscle, insulin-stimulated phosphorylation of Akt on Ser473 remained unaltered by the HFD in transgenic mice, whereas the insulin response was blunted in wild-type mice (Fig. 6*E*). Therefore, these results indicated that transgenic mice fed an HFD remained glucose-tolerant and insulin-sensitive.

VEGF overexpression increases M2 anti-inflammatory macrophages and reduces M1 proinflammatory macrophages in adipose tissue. In addition to inducing angiogenesis, VEGF is involved in macrophage recruitment (25). In wild-type mice, cells positive for the macrophage marker MAC-2 were only detected in BAT and WAT under HFD conditions (Fig. 7*A*). In contrast, transgenic mice fed an HFD or chow presented MAC-2–positive cells in both WAT and BAT (Fig. 7*A*). The population of the infiltrate was further analyzed by flow cytometry analysis. Accordingly, the percentage of $CD11b^{+}F480^{+}$ cells was lower in wild-type mice fed chow than in all the other groups (Fig. 7*B*). The percentage of $MHCII^{+}CD11b^{+}$ and $MHCII^{+}CD11c^{+}$ double-positive cells was increased in HFD-fed wild-type mice but not in transgenic mice (Fig. 7*C* and *D*), indicating that the HFD induced a higher capacity for antigen presentation in macrophages and dendritic cells of wild-type mice. Moreover, transgenic mice fed both chow and the HFD presented lower M1 proinflammatory macrophages (decreased $CD11c^{high}$ $F4/80^{+}$ cells; Fig. 7*E*) and an increase in M2 anti-inflammatory macrophages (increased $MGL1^{+}CD11b^{+}$ cells; Fig. 7*F*).

The enrichment of M2 vs M1 macrophages in the WAT of transgenic mice could influence the profile of proinflammatory cytokines production. Indeed, levels of leptin and MCP-1 were dramatically increased in wild-type mice fed an HFD but were only slightly increased in transgenic mice (Fig. 8*A*–*D*). Similarly, the WAT of wild-type but not transgenic mice presented increased IFN-γ protein levels under the HFD (Fig. 8*E*). In addition, transgenic mice had lower IL-6 and TNF-α WAT protein levels (Fig. 8*F* and *G*). In contrast, levels of the anti-inflammatory adipokine, adiponectin, remained unchanged in all groups (Fig. 8*H* and *I*).

To examine whether VEGF could switch macrophages to the M2 phenotype, BMDMs were treated with VEGF; however, this treatment did not lead to an increase in M2

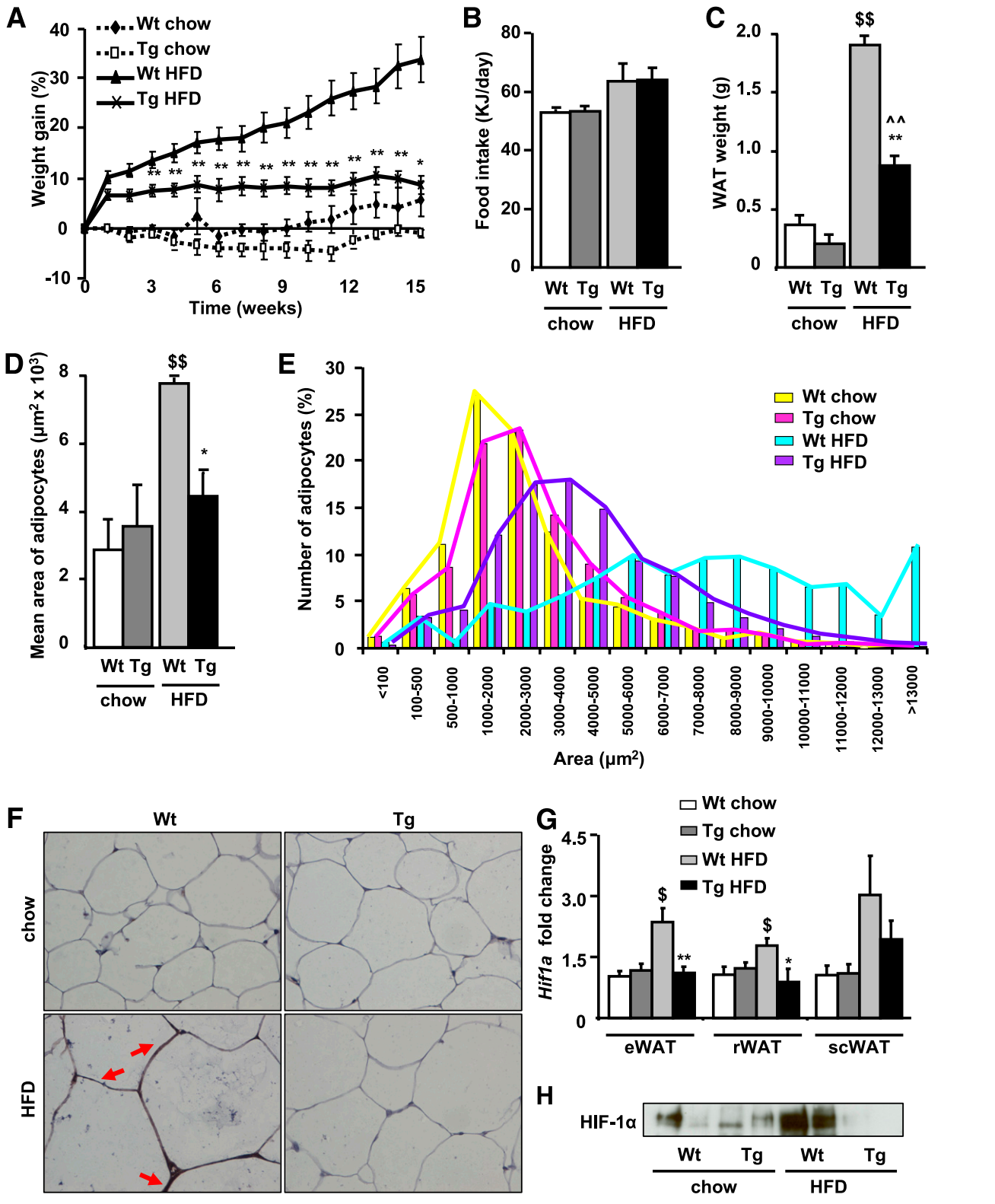

FIG. 2. Reduced adiposity in aP2VEGF transgenic (Tg) mice fed an HFD. Weight gain (*A*) and food intake (*B*), calculated as estimated metabolisable energy of wild-type (Wt) and Tg mice fed chow or an HFD for 15 weeks. Data represent the mean ± SEM of at least 10 animals per group. *C*: Epididymal WAT weight. *D*: Mean adipocyte area. *E*: Frequency distribution of adipocyte area in Wt and Tg mice fed chow or an HFD. Data represent the mean ± SEM of at least four animals per group. *F*: Representative hypoxyprobe sections of epididymal WAT, counterstained with hematoxylin (original magnification ×400). Red arrows indicate hypoxyprobe signal. *G*: *Hif1a* expression was analyzed by quantitative real-time PCR in epididymal WAT (eWAT), retroperitoneal WAT (rWAT), and subcutaneous WAT (scWAT), and was normalized by *36B4* expression. Data represent the mean ± SEM of at least seven animals per group. *H*: Representative WAT Western blot blotted with an antibody against HIF-1α. *P < 0.05 vs. Wt HFD. **P < 0.01 vs. Wt HFD. \$$P$ < 0.05 vs. Wt chow. \$\$$P$ < 0.01 vs. Wt chow. ^^P < 0.01 vs. Tg chow. (A high-quality digital representation of this figure is available in the online issue.)

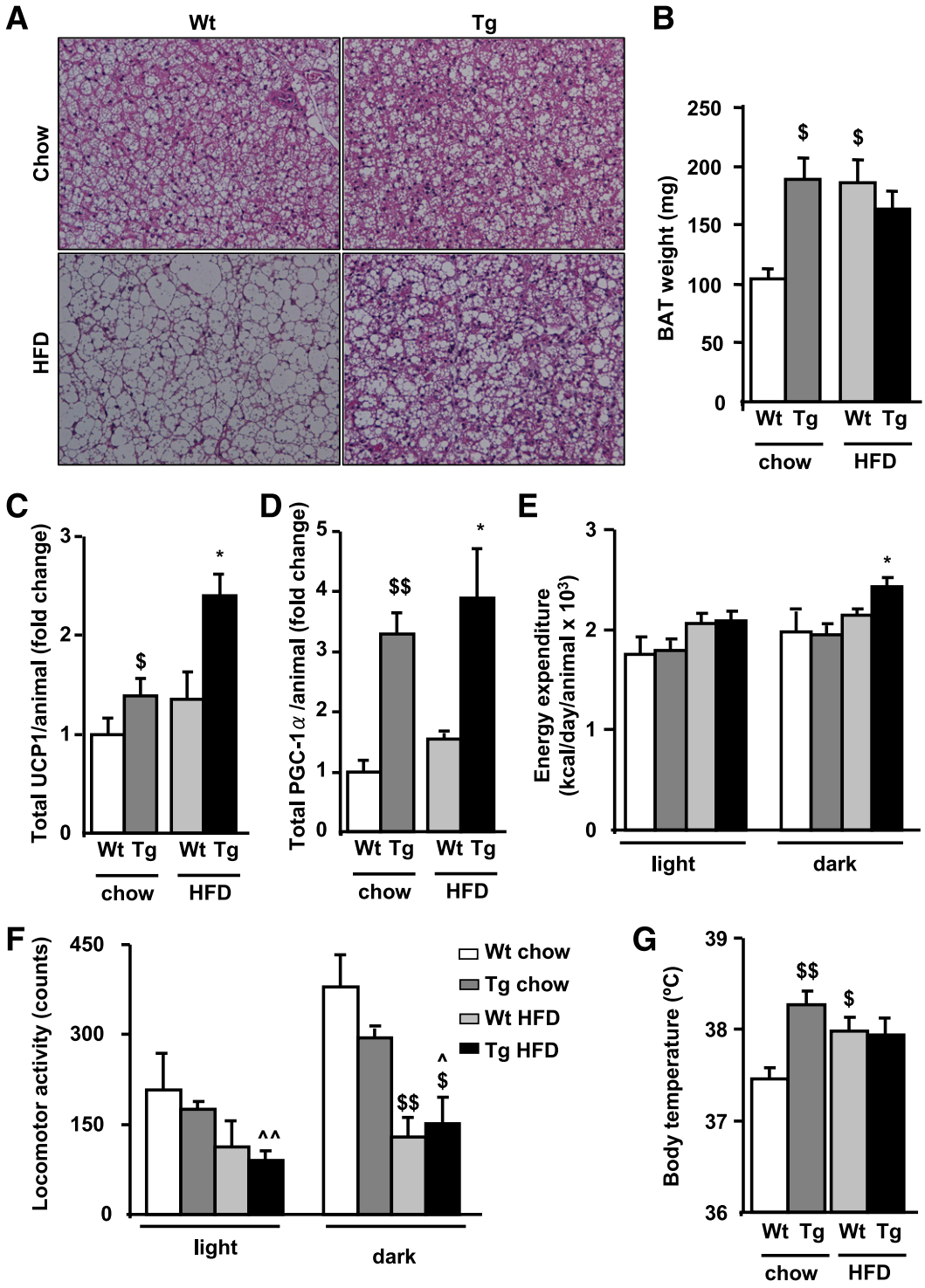

FIG. 3. Transgenic (Tg) mice showed increased BAT thermogenesis and energy expenditure. *A*: Representative sections of BAT, stained with hematoxylin-eosin (original magnification ×200) for Tg and wild-type (Wt) mice. *B*: Interscapular BAT tissue weight. Data represent the mean ± SEM of at least 10 animals per group. Total content of UCP1 (*C*) and PGC-1α (*D*) were determined by Western blot densitometry, taking into account the amount of total BAT protein. Data represent the mean ± SEM of at least four animals per group. Energy expenditure (*E*) and locomotor activity (*F*) was measured with an indirect open circuit calorimeter in Wt and Tg mice fed chow or an HFD for 15 weeks. Data were taken during the light and dark cycles and represent the mean ± SEM of at least eight animals per group. *G*: Body temperature was measured in awake animals using an intrarectal probe. Data represent the mean ± SEM of at least 10 animals per group. *$P < 0.05$ vs. Wt HFD. \$$P < 0.05$ vs. Wt chow. \$\$$P < 0.01$ vs. Wt chow. ^$P < 0.05$ vs. Tg chow. ^^$P < 0.01$ vs. Tg chow. (A high-quality digital representation of this figure is available in the online issue.)

markers such as *Arg1* or *Il10* (Fig. 8*J* and *K*). Because VEGF receptor 2 (VEGFR2) (*Kdr*) together with the chemokine stromal cell-derived factor (SDF)-1 (*Cxcl12*) are involved in VEGF-induced macrophage mobilization and retention in adipose tissue (26), expression of *Kdr* in macrophages and *Cxcl12* in adipose tissue was examined. In transgenic mice, *Kdr* and *Cxcl12* expression were both increased compared with wild-type mice (Fig. 8*L* and *M*).

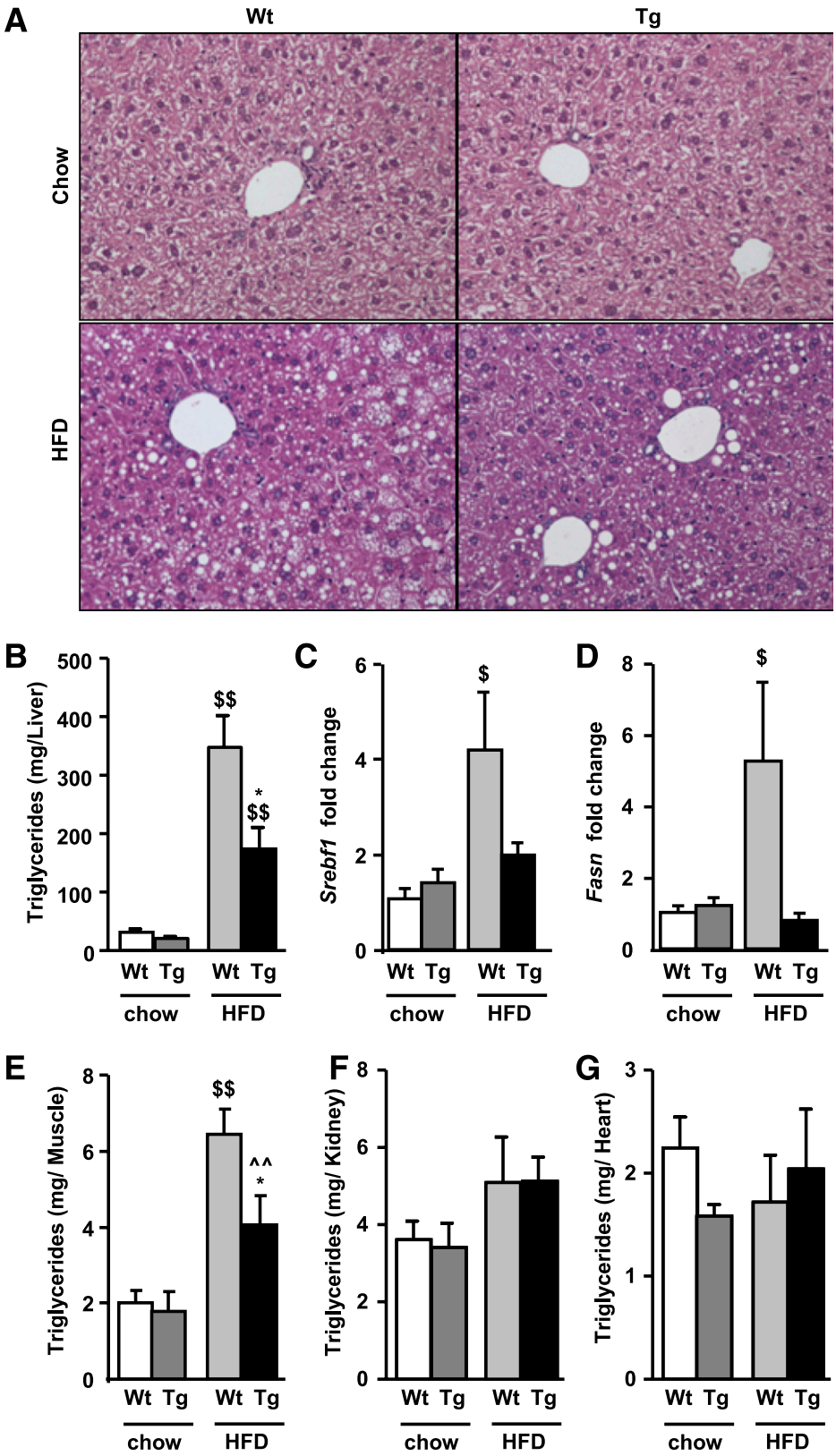

FIG. 4. Transgenic (Tg) mice showed decreased hepatic fat accumulation compared with wild-type (Wt) mice. *A*: Representative sections of liver, stained with hematoxylin-eosin (original magnification ×400). *B*: Liver triglyceride content was determined as indicated in RESEARCH DESIGN AND METHODS. *Srebf1* (*C*) and *Fasn* (*D*) liver expression were analyzed by quantitative real-time PCR and normalized by *36B4* expression. Triglyceride content was determined in muscle (*E*), kidney (*F*), and heart (*G*) as indicated in RESEARCH DESIGN AND METHODS. Data represent the mean ± SEM of at least 10 animals per group. **P* < 0.05 vs. Wt HFD. $*P* < 0.05 vs. Wt chow. $$*P* < 0.01 vs. Wt chow. ^^*P* < 0.01 vs. Tg chow. (A high-quality digital representation of this figure is available in the online issue.)

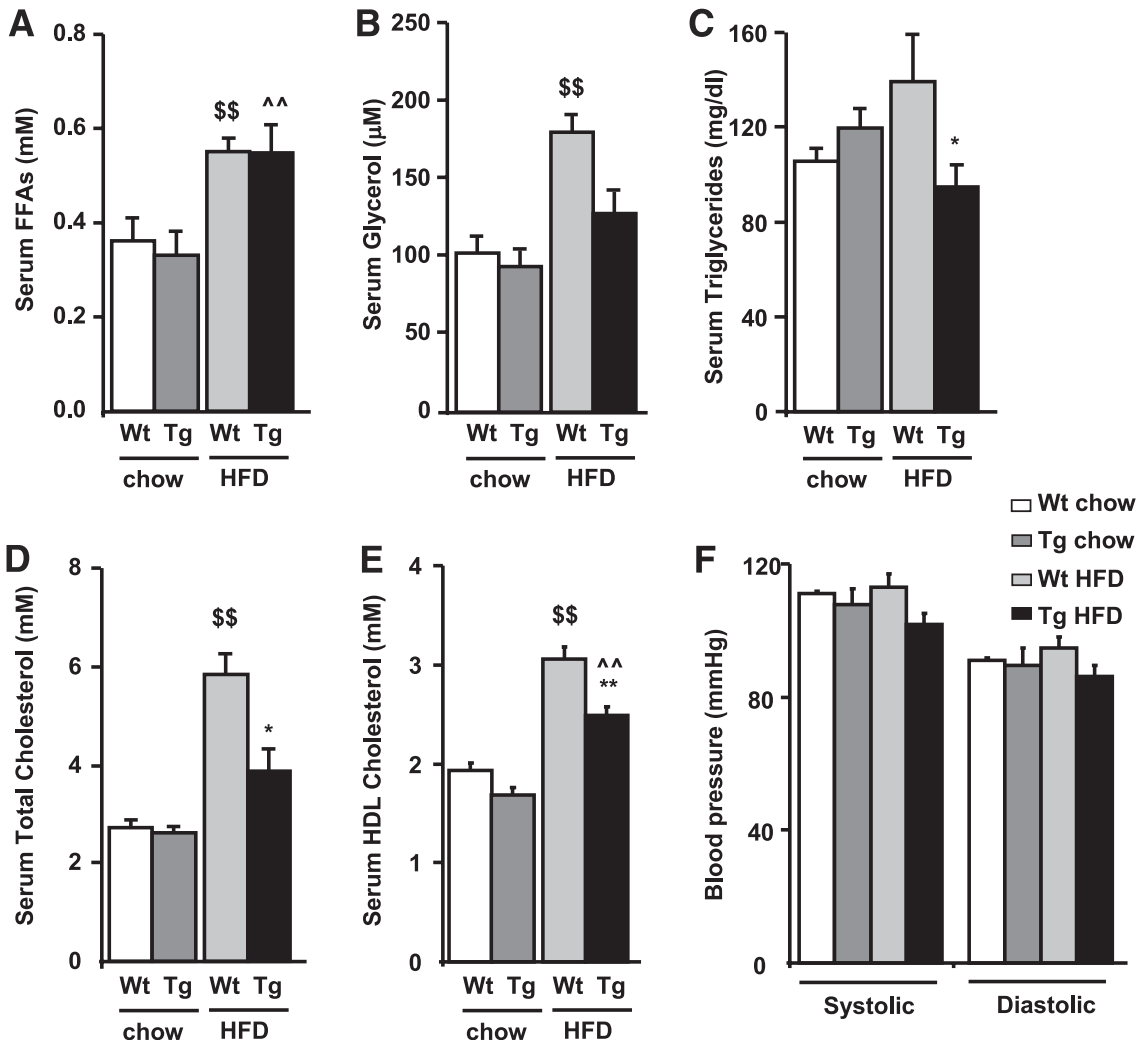

FIG. 5. Levels of circulating metabolites and blood pressure were determined in transgenic (Tg) and wild-type (Wt) mice fed chow and HFD. Serum levels of FFAs (*A*), glycerol (*B*), triglycerides (*C*), total cholesterol (*D*), and HDL cholesterol (*E*) were analyzed, and systolic and diastolic blood pressure (*F*) was determined as indicated in RESEARCH DESIGN AND METHODS. Data represent the mean ± SEM of at least 10 animals per group. **P* < 0.05 vs. Wt HFD. ***P* < 0.01 vs. Wt HFD. $$*P* < 0.01 vs. Wt chow. ^^*P* < 0.01 vs. Tg chow.

These results suggest that VEGF may attract M2 macrophages in adipose tissue through macrophage-VEGFR2 and SDF1.

DISCUSSION

Studies have reported that angiogenesis fails to maintain normoxia in adipose depots and that local hypoxia occurs in obesity (4,5). Thus, it has been hypothesized that this reduction in adipose tissue blood flow may trigger insulin resistance. To examine whether an increase in adipose tissue angiogenesis could protect against insulin resistance, transgenic mice overexpressing VEGF in adipose tissue were generated. Although adipose tissue angiogenesis can be promoted by several factors, such as leptin, HIF-1α, or VEGF, overexpression of leptin in adipose tissue failed to induce angiogenesis (27), and transgenic mice with dominant, active HIF-1α presented fibrosis but not vessel growth (28). Our study showed that overexpression of $VEGF_{164}$ was able to induce vessel formation in both WAT and BAT. Moreover, fluorescein angiographies and electron microscopy studies both showed that these blood vessels were functional and more dilated. In accordance with our results, other studies in which $VEGF_{164}$ was expressed demonstrated the ability of this isoform to induce the development of new vessels (29). Furthermore, we did not observe an increase in vessel density in nonadipose tissues of the transgenic mice. Indeed, to enhance angiogenesis, the correct relationship between VEGF gradient and concentration is determinant (30), and in our transgenic mice, this may only be present in the site of production.

To our knowledge, this is the first time that the effects of increased angiogenesis on adipose tissue growth and insulin resistance have been studied. However, because it is well established that the expansion of adipose tissue is supported by angiogenesis (31), several studies have developed antiangiogenesis approaches to achieve a therapeutic intervention of obesity. Administration of angiogenic inhibitors to obese mice has resulted in decreased adipose tissue mass and concomitant weight loss (17,32,33). Although the inhibition of angiogenesis seems to prevent the expansion of adipose tissue mass, our results demonstrate that an increase in vessel density does not result in an increase in the mass of WAT.

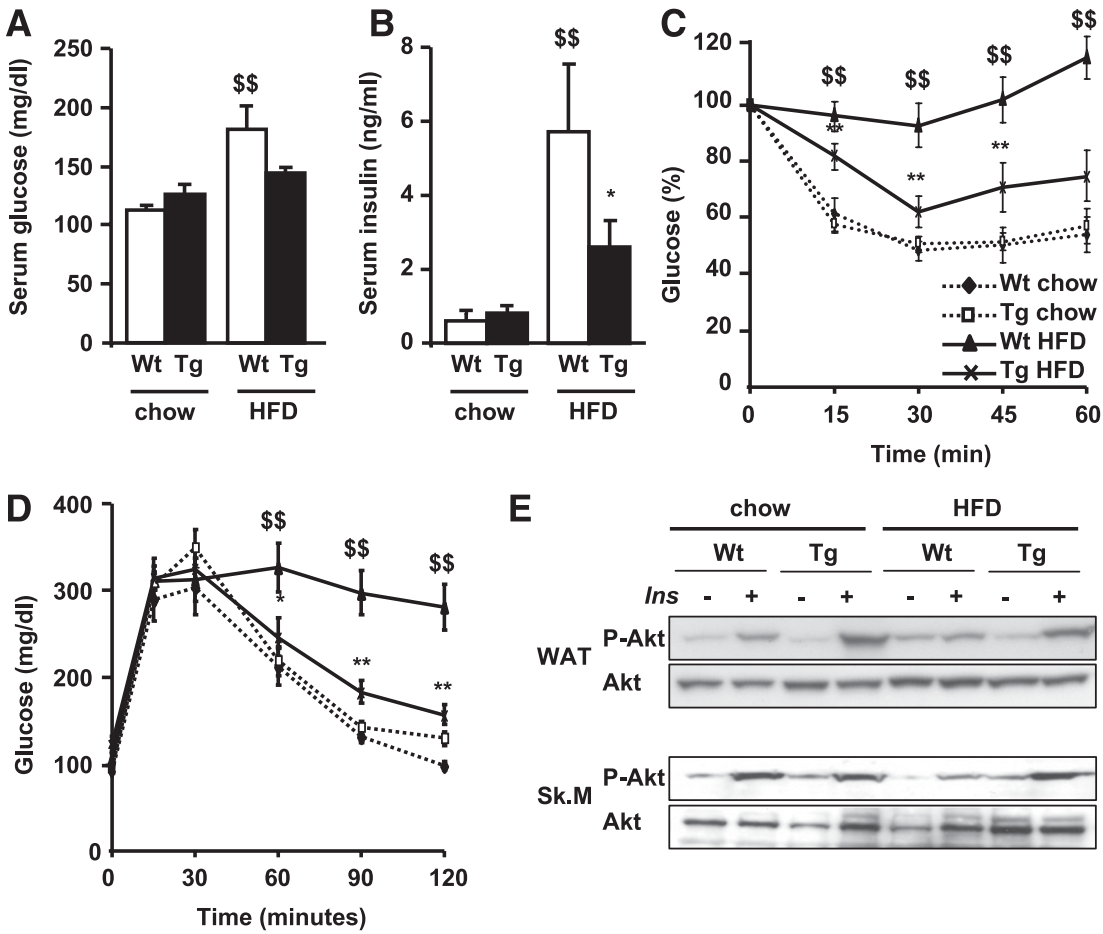

FIG. 6. aP2VEGF transgenic (Tg) mice are protected against diet-induced glucose intolerance and insulin resistance compared with wild-type (Wt) mice. Blood glucose (*A*) and insulin (*B*) levels are shown in chow and HFD-fed mice. Data represent the mean ± SEM of at least 10 animals per group. *C*: Insulin sensitivity was determined after an intraperitoneal injection of insulin (0.75 units/kg body weight). Results are calculated as the percentage of initial blood glucose levels. Data represent the mean ± SEM of at least eight animals per group. *D*: Glucose tolerance was determined in fasted mice after an intraperitoneal injection of glucose (2 g/kg body weight), and blood glucose levels were measured at the indicated time points. Data represent the mean ± SEM of at least eight animals per group. *E*: Representative Western blots are shown for total Akt and phosphorylated Akt (p-Akt) levels in WAT and skeletal muscle (Sk.M) before and after insulin stimulation in chow- and HFD-fed mice, as indicated in RESEARCH DESIGN AND METHODS. *$P < 0.05$ vs. Wt HFD. **$P < 0.01$ vs. Wt HFD. \$\$$P < 0.01$ vs. Wt chow.

Noticeably, the protection against HFD-induced obesity of transgenic mice could be explained by the enhanced energy expenditure and the increase in total protein levels of key genes involved in thermogenesis and mitochondrial biogenesis in BAT, such as UCP1 and PGC-1α (34). In accordance with our studies, transgenic mice overexpressing UCP1 in adipose tissue are protected against HFD-induced obesity (35). Moreover, the greater BAT vessel density of transgenic mice may be comparable to that observed during cold exposure. Indeed, cold exposure enhances BAT angiogenesis in a hypoxia-independent but VEGF-dependent process (36), and increased BAT vessel density enables higher rate of blood perfusion to supply oxygen and FFAs and to facilitate heat dissipation, all of them necessary for UCP1-induced thermogenesis. Taken together, our data suggest that increased vascularization in the BAT of transgenic mice increases BAT size and enhances UCP1 expression and thermogenesis. Thus, phenotypic changes in the body weight of aP2VEGF transgenic mice may be attributed to the increased energy expenditure and thermogenic activity of BAT. Furthermore, recent studies suggest that BAT is more abundant in adult humans than previously recognized (37–40). As a consequence, strategies aimed at stimulating the generation and/or activation of BAT, such as enhancing BAT angiogenesis, might lead to new approaches to counteract obesity.

Transgenic mice were protected not only against HFD-induced obesity but also systemic insulin resistance. Glucose tolerance and insulin sensitivity were both improved in transgenic mice. The absence of insulin resistance in these mice may be linked not only to a lack of fat accumulation but also to decreased infiltration of proinflammatory macrophages. It is well accepted that adipose tissue contains BMDMs and that the content of these macrophages correlates with the degree of obesity and insulin resistance (12,41). Strikingly, despite being neither obese nor insulin resistant, transgenic mice presented significant macrophage infiltration when fed not only an HFD but also the chow diet. However, flow cytometry analysis indicated lower M1 proinflammatory and increased M2 anti-inflammatory macrophages in the adipose tissue of aP2VEGF transgenic mice.

Our current understanding of how adipose tissue macrophages promote obesity-associated insulin resistance is based on the model proposed by Lumeng et al. (13), in which the recruitment of M1 macrophages promotes the

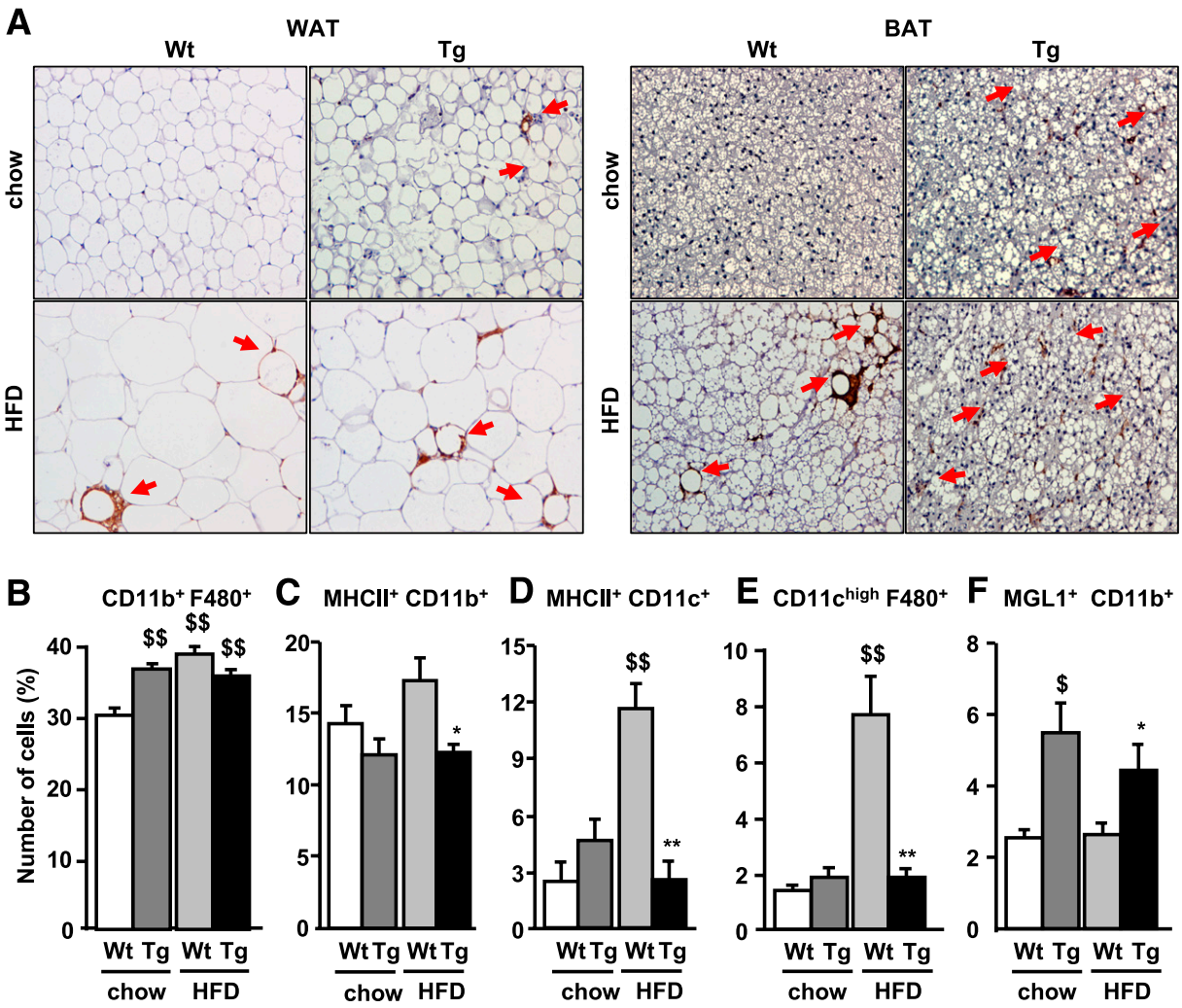

FIG. 7. Study of WAT and BAT infiltrates. *A*: MAC-2 immunohistochemistry was performed in WAT and BAT of wild-type (Wt) and transgenic (Tg) mice (representative images at original magnification ×200). Red arrows indicate MAC-2 signal. Flow cytometry analysis of CD11b$^+$ F480$^+$ (*B*), MHCII$^+$ CD11b$^+$ (*C*), MHCII$^+$ CD11c$^+$ (*D*), CD11c^{high} F4/80$^+$ (*E*), and MGL1$^+$ CD11b$^+$ (*F*) cells in WAT. The stroma vascular fraction from Wt and Tg mice fed chow or an HFD was double incubated with corresponding antibodies to detect different cell populations. Data represent the mean ± SEM of at least five animals for each group. *$P < 0.05$ vs. Wt HFD. **$P < 0.01$ vs. Wt HFD. \$$P < 0.05$ vs. Wt chow. \$\$$P < 0.01$ vs. Wt chow. (A high-quality digital representation of this figure is available in the online issue.)

change of the anti-inflammatory milieu maintained by M2 macrophages toward an inflammatory state. Therefore, the decrease in M1 proinflammatory and increased presence of M2 anti-inflammatory macrophages in adipose tissue of our mice may be protecting them from insulin resistance. In line with our studies, the ablation of CD11c$^+$ cells in mice leads to a marked reduction in proinflammatory cytokines and an improvement of insulin sensitivity (42). Furthermore, selective inactivation of peroxisome proliferator–activated receptor (PPAR)-γ in macrophages results in an impairment of M2 macrophages maturation, leading to insulin resistance and glucose intolerance (43). The amount of dendritic cells and macrophages positive for MHCII was also reduced. MHCII is often linked with increased inflammatory response. Indeed, MHCII knockout mice exhibit reduced secretion of proinflammatory cytokines in macrophages (44). In accordance with the reduced infiltration by M1 macrophages, the expression of adipose tissue proinflammatory cytokines, such as leptin, IFN-γ, MCP-1, IL-6, and TNF-α, was reduced in HFD-fed transgenic mice compared with wild-type mice. This decrease may, in turn, have led to lower grade of adipose tissue M1 macrophage infiltration. Therefore, the reduction of M1 adipose tissue macrophages and the lower proinflammatory cytokine secretion in our mice may protect them from the development of insulin resistance.

We demonstrate that VEGF enhances the presence of M2 anti-inflammatory macrophages in the adipose tissue of these mice. However, whether VEGF acts as a specific chemotactic for M2 macrophages in adipose tissue or promotes macrophage polarization switch toward an M2 phenotype remains unclear. The inability of VEGF to increase the expression of M2 markers in BMDMs suggests that VEGF alone is not able to induce the switch toward the M2 phenotype. Recent studies have demonstrated that another cytokine, adiponectin, is able to promote macrophage polarization toward an M2 phenotype (45,46). However, adiponectin levels remained unchanged in our model, thus excluding a role of this adipokine in the transgenic phenotype. This suggests that VEGF is probably attracting M2 macrophages to adipose tissue. Consistent with this, VEGF plays a major role in wound repair and angiogenesis, processes likely involving mobilization of M2 macrophages (47,48). In addition, VEGF enhances

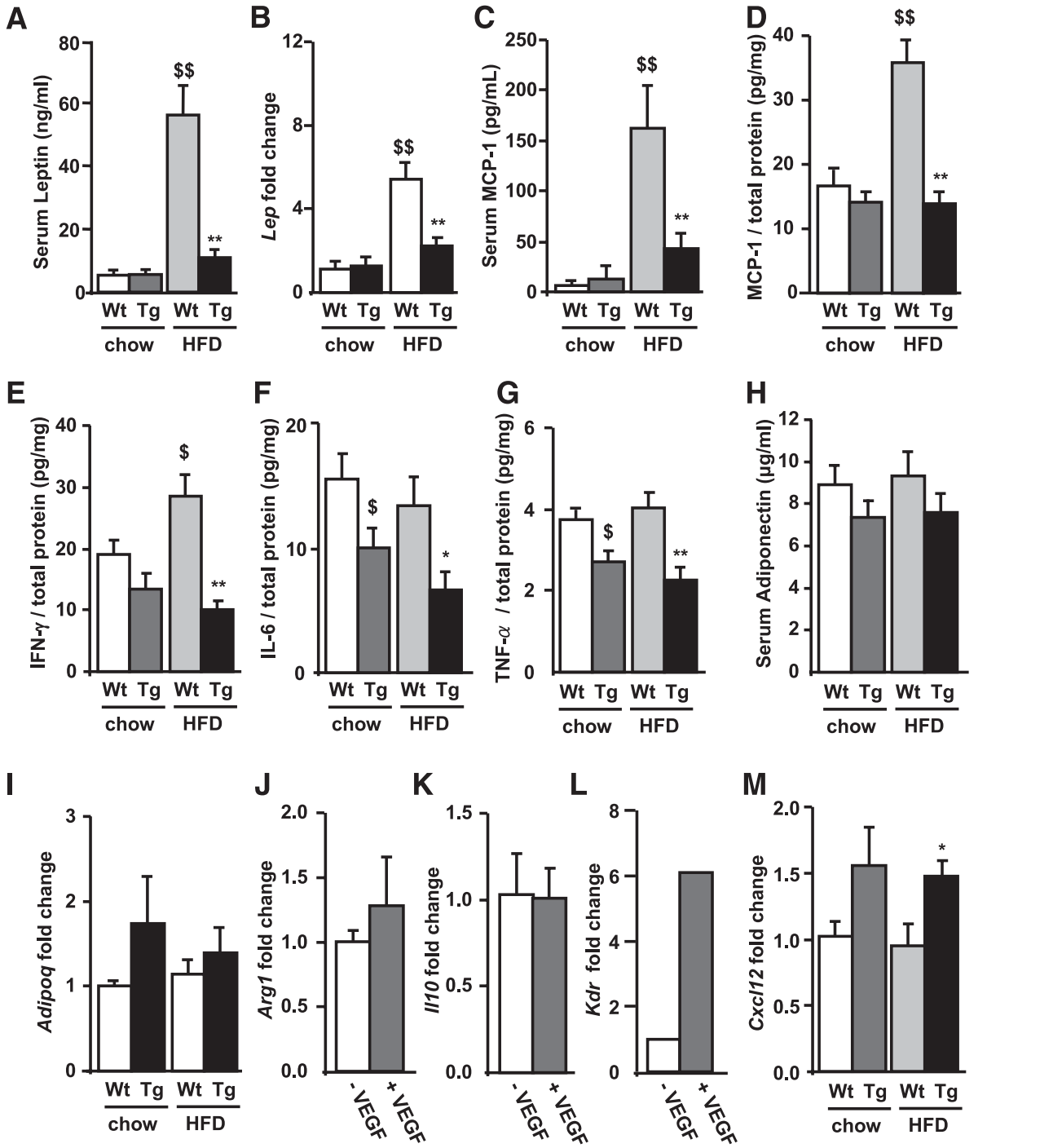

FIG. 8. Effects of VEGF on macrophage phenotype in transgenic (Tg) and wild-type (Wt) mice. *A*: Serum leptin levels were determined by enzyme-linked immunosorbent assay (ELISA) as indicated in RESEARCH DESIGN AND METHODS. *B*: *Lep* expression in WAT was analyzed by quantitative real-time PCR and normalized by *36B4* expression. *C*: Serum MCP-1 levels were determined by ELISA as indicated in RESEARCH DESIGN AND METHODS. *D*: Protein MCP-1 levels in WAT were analyzed by Luminex and calculated as MCP-1 per total protein. WAT IFN-γ (*E*), IL-6 (*F*), and TNF-α (*G*) levels were determined by Luminex, as indicated in RESEARCH DESIGN AND METHODS, and results were calculated per total protein. *H*: Serum adiponectin levels were determined by radioimmunoassay, as indicated in RESEARCH DESIGN AND METHODS. *I*: *Adipoq* expression in WAT was analyzed by quantitative real-time PCR and normalized by *36B4* expression. BMDMs of Wt mice were treated with or without VEGF and *Arg1* (*J*), *Il10* (*K*), and *Kdr* (*L*) expression levels were determined by quantitative real-time PCR and normalized by *36B4* expression. *M*: WAT *Cxcl12* expression was analyzed by quantitative real-time PCR and normalized by *36B4* expression. Data represent the mean ± SEM of at least 10 animals per group. **P* < 0.05 vs. Wt HFD. ***P* < 0.01 vs. Wt HFD. $*P* < 0.05 vs. Wt chow. $$*P* < 0.01 vs. Wt chow.

angiogenesis in adipose tissue by inducing macrophage recruitment and retention through its receptor VEGFR2 (*Kdr*) (26). The chemokine SDF-1 *(Cxcl12)* is critical in this process (26). Moreover, SDF-1 is upregulated by VEGF (49). In agreement with this, expression of macrophage *Kdr* and adipose tissue *Cxcl12* were both increased in aP2VEGF mice, suggesting that the increase in M2 macrophages is due to the chemotactic activity of VEGF. Altogether, these results suggest that VEGF may attract M2 macrophages to adipose tissue through VEGFR2 and SDF1.

In summary, we show that overexpression of VEGF displays beneficial effects. In BAT, our results highlight the crucial role of vascularization in promoting its size and thermogenesis as a means to counteract the development of HFD-induced obesity. In WAT, the increase of angiogenesis promoted by VEGF overexpression did not lead to an increase in adipose tissue mass. Moreover, adipose tissue from animals overexpressing VEGF presented increased recruitment of M2 anti-inflammatory macrophages, thus maintaining an anti-inflammatory milieu and avoiding insulin resistance. Therefore, targeting VEGF expression in adipose tissue may offer the opportunity for a novel therapeutic approach to prevent or even treat the progression of obesity-related insulin resistance.

ACKNOWLEDGMENTS

This work was supported by grants from the Ministerio de Ciencia e Innovación, Plan Nacional I+D+I (SAF2008-00962) and Generalitat de Catalunya (2009 SGR-224), Spain, and the European Community's FP6 EUGENE2 (LSHM-CT-2004-512013) and EUMODIC (LSHG-CT-2006-037188). L.V. received postdoctoral fellowship Juan de la Cierva (Ministerio de Ciencia e Innovacion).

No potential conflicts of interest relevant to this article were reported.

I.E. and S.F. conceived the experiments, researched data, contributed to discussion, and wrote the manuscript. T.F. researched data and contributed to discussion. L.V., S.T., S.M., C.R., D.R., A.P., E.R., and J.R. researched data. F.B. conceived the experiments, contributed to discussion, and wrote the manuscript. F.B. is the guarantor of this work and, as such, had full access to all the data in the study and takes responsibility for the integrity of the data and the accuracy of the data analysis.

The authors thank Drs. Malcolm Watford (Rutgers University) and Virginia Haurigot (Universitat Autònoma de Barcelona) for helpful discussion and Marta Moya (Universitat Autònoma de Barcelona) and Mireia Zaguirre (Universitat Autònoma de Barcelona) for technical assistance.

REFERENCES

1. Cornier MA, Dabelea D, Hernandez TL, et al. The metabolic syndrome. Endocr Rev 2008;29:777–822
2. James WP. The epidemiology of obesity: the size of the problem. J Intern Med 2008;263:336–352
3. Rutkowski JM, Davis KE, Scherer PE. Mechanisms of obesity and related pathologies: the macro- and microcirculation of adipose tissue. FEBS J 2009;276:5738–5746
4. Hosogai N, Fukuhara A, Oshima K, et al. Adipose tissue hypoxia in obesity and its impact on adipocytokine dysregulation. Diabetes 2007;56:901–911
5. Rausch ME, Weisberg S, Vardhana P, Tortoriello DV. Obesity in C57BL/6J mice is characterized by adipose tissue hypoxia and cytotoxic T-cell infiltration. Int J Obes (Lond) 2008;32:451–463
6. Pasarica M, Sereda OR, Redman LM, et al. Reduced adipose tissue oxygenation in human obesity: evidence for rarefaction, macrophage chemotaxis, and inflammation without an angiogenic response. Diabetes 2009;58:718–725
7. Ye J, Gao Z, Yin J, He Q. Hypoxia is a potential risk factor for chronic inflammation and adiponectin reduction in adipose tissue of ob/ob and dietary obese mice. Am J Physiol Endocrinol Metab 2007;293:E1118–E1128
8. Trayhurn P, Wood IS. Adipokines: inflammation and the pleiotropic role of white adipose tissue. Br J Nutr 2004;92:347–355
9. Trayhurn P, Wang B, Wood IS. Hypoxia and the endocrine and signalling role of white adipose tissue. Arch Physiol Biochem 2008;114:267–276
10. Wang B, Wood IS, Trayhurn P. Dysregulation of the expression and secretion of inflammation-related adipokines by hypoxia in human adipocytes. Pflugers Arch 2007;455:479–492
11. Neels JG, Olefsky JM. Inflamed fat: what starts the fire? J Clin Invest 2006; 116:33–35
12. Xu H, Barnes GT, Yang Q, et al. Chronic inflammation in fat plays a crucial role in the development of obesity-related insulin resistance. J Clin Invest 2003;112:1821–1830
13. Lumeng CN, Bodzin JL, Saltiel AR. Obesity induces a phenotypic switch in adipose tissue macrophage polarization. J Clin Invest 2007;117:175–184
14. Shoelson SE, Lee J, Goldfine AB. Inflammation and insulin resistance. J Clin Invest 2006;116:1793–1801
15. Virtue S, Vidal-Puig A. Adipose tissue expandability, lipotoxicity and the metabolic syndrome—an allostatic perspective. Biochim Biophys Acta 2010;1801:338–349
16. Carmeliet P. Angiogenesis in health and disease. Nat Med 2003;9:653–660
17. Neels JG, Thinnes T, Loskutoff DJ. Angiogenesis in an in vivo model of adipose tissue development. FASEB J 2004;18:983–985
18. Roy H, Bhardwaj S, Ylä-Herttuala S. Biology of vascular endothelial growth factors. FEBS Lett 2006;580:2879–2887
19. Loebig M, Klement J, Schmoller A, et al. Evidence for a relationship between VEGF and BMI independent of insulin sensitivity by glucose clamp procedure in a homogenous group healthy young men. PLoS ONE 2010;5:e12610
20. Franckhauser S, Muñoz S, Elias I, Ferre T, Bosch F. Adipose overexpression of phosphoenolpyruvate carboxykinase leads to high susceptibility to diet-induced insulin resistance and obesity. Diabetes 2006;55:273–280
21. Muñoz S, Franckhauser S, Elias I, et al. Chronically increased glucose uptake by adipose tissue leads to lactate production and improved insulin sensitivity rather than obesity in the mouse. Diabetologia 2010;53:2417–2430
22. García M, Pujol A, Ruzo A, et al. Phosphofructo-1-kinase deficiency leads to a severe cardiac and hematological disorder in addition to skeletal muscle glycogenosis. PLoS Genet 2009;5:e1000615
23. Carr TP, Andresen CJ, Rudel LL. Enzymatic determination of triglyceride, free cholesterol, and total cholesterol in tissue lipid extracts. Clin Biochem 1993;26:39–42
24. Bruscia EM, Zhang PX, Satoh A, et al. Abnormal trafficking and degradation of TLR4 underlie the elevated inflammatory response in cystic fibrosis. J Immunol 2011;186:6990–6998
25. Yang ZF, Poon RT, Luo Y, et al. Up-regulation of vascular endothelial growth factor (VEGF) in small-for-size liver grafts enhances macrophage activities through VEGF receptor 2-dependent pathway. J Immunol 2004; 173:2507–2515
26. Cho CH, Koh YJ, Han J, et al. Angiogenic role of LYVE-1-positive macrophages in adipose tissue. Circ Res 2007;100:e47–e57
27. Wator L, Razny U, Balwierz A, et al. Impaired leptin activity in New Zealand Obese mice: model of angiogenesis. Genes Nutr 2008;3:177–180
28. Halberg N, Khan T, Trujillo ME, et al. Hypoxia-inducible factor 1alpha induces fibrosis and insulin resistance in white adipose tissue. Mol Cell Biol 2009;29:4467–4483
29. Pettersson A, Nagy JA, Brown LF, et al. Heterogeneity of the angiogenic response induced in different normal adult tissues by vascular permeability factor/vascular endothelial growth factor. Lab Invest 2000;80:99–115
30. Gerhardt H. VEGF and endothelial guidance in angiogenic sprouting. Organogenesis 2008;4:241–246
31. Cao Y. Angiogenesis modulates adipogenesis and obesity. J Clin Invest 2007;117:2362–2368
32. Bråkenhielm E, Cao R, Gao B, et al. Angiogenesis inhibitor, TNP-470, prevents diet-induced and genetic obesity in mice. Circ Res 2004;94: 1579–1588
33. Rupnick MA, Panigrahy D, Zhang CY, et al. Adipose tissue mass can be regulated through the vasculature. Proc Natl Acad Sci U S A 2002;99: 10730–10735
34. Cannon B, Nedergaard J. Brown adipose tissue: function and physiological significance. Physiol Rev 2004;84:277–359
35. Kopecký J, Hodný Z, Rossmeisl M, Syrový I, Kozak LP. Reduction of dietary obesity in aP2-Ucp transgenic mice: physiology and adipose tissue distribution. Am J Physiol 1996;270:E768–E775
36. Xue Y, Petrovic N, Cao R, et al. Hypoxia-independent angiogenesis in adipose tissues during cold acclimation. Cell Metab 2009;9:99–109
37. Cypess AM, Lehman S, Williams G, et al. Identification and importance of brown adipose tissue in adult humans. N Engl J Med 2009;360:1509–1517
38. Nedergaard J, Bengtsson T, Cannon B. Unexpected evidence for active brown adipose tissue in adult humans. Am J Physiol Endocrinol Metab 2007;293:E444–E452
39. van Marken Lichtenbelt WD, Vanhommerig JW, Smulders NM, et al. Cold-activated brown adipose tissue in healthy men. N Engl J Med 2009;360: 1500–1508
40. Virtanen KA, Lidell ME, Orava J, et al. Functional brown adipose tissue in healthy adults. N Engl J Med 2009;360:1518–1525
41. Weisberg SP, McCann D, Desai M, Rosenbaum M, Leibel RL, Ferrante AW Jr. Obesity is associated with macrophage accumulation in adipose tissue. J Clin Invest 2003;112:1796–1808

42. Patsouris D, Li PP, Thapar D, Chapman J, Olefsky JM, Neels JG. Ablation of CD11c-positive cells normalizes insulin sensitivity in obese insulin resistant animals. Cell Metab 2008;8:301–309
43. Odegaard JI, Ricardo-Gonzalez RR, Goforth MH, et al. Macrophage-specific PPARgamma controls alternative activation and improves insulin resistance. Nature 2007;447:1116–1120
44. Frei R, Steinle J, Birchler T, et al. MHC class II molecules enhance Toll-like receptor mediated innate immune responses. PLoS ONE 2010;5:e8808
45. Ohashi K, Parker JL, Ouchi N, et al. Adiponectin promotes macrophage polarization toward an anti-inflammatory phenotype. J Biol Chem 2010; 285:6153–6160
46. Lovren F, Pan Y, Quan A, et al. Adiponectin primes human monocytes into alternative anti-inflammatory M2 macrophages. Am J Physiol Heart Circ Physiol 2010;299:H656–H663
47. Deonarine K, Panelli MC, Stashower ME, et al. Gene expression profiling of cutaneous wound healing. J Transl Med 2007;5:11
48. Fantin A, Vieira JM, Gestri G, et al. Tissue macrophages act as cellular chaperones for vascular anastomosis downstream of VEGF-mediated endothelial tip cell induction. Blood 2010;116:829–840
49. Urao N, Razvi M, Oshikawa J, et al. IQGAP1 is involved in post-ischemic neovascularization by regulating angiogenesis and macrophage infiltration. PLoS ONE 2010;5:e13440